Vertical-Cavity Surface-Emitting Lasers With Two Emission-Controllable Transverse Modes

Chuyu Zhong, Xing Zhang, *Member, IEEE*, Lijuan Yu, Jian Guo Liu, Werner Hofmann, *Member, IEEE*, Yongqiang Ning, and Lijun Wang

***Abstract*— We propose a vertical-cavity surface-emitting laser (VCSEL) with two transverse modes independently controlled by two contacts. By directly etching a trench in the p-doped distributed Bragg reflector, we form an air gap and two sub-mesas as waveguides above the oxide layer. Contacts are deposited on each sub-mesa. Emission control on two different spatial modes in a single VCSEL is achieved by changing the driving condition of one-contact or two-contact injection. Owing to this feature, the proposed VCSEL has a potential as a cost-effective source for optical communications using spatial-division multiplexing.**

***Index Terms*— Few mode, VCSEL, air gap, mode control, independent contact.**

I. Introduction

VERTICAL-cavity surface-emitting lasers (VCSELs) own many attractive optical and electrical properties, such as single-longitudinal-mode emission, low-threshold current, low-divergence circular output beam, high stability and high-speed modulation, making VCSELs a key component for optical communications [1], [2].

In optical communications systems employing spatial-division multiplexing (SDM) [3]–[5], a technology expected to overcome the "capacity crunch" of present-day communications [6]–[8], VCSELs are employed in the form of arrays as they are in other multiplexing technologies [9], [10]. The optical signals of different VCSELs need to be combined from a bundle of single-mode fibers into different modes or separate cores of an SDM fiber by spatial multiplexers (SMUXs) [11].

The fact that a single VCSEL can support many transverse modes through its large transverse dimensions is neglected to a certain extent. The optical modes in an oxidized VCSEL are governed by the complex interplay among multiple effects [12]–[14], including carrier confinement, modal losses, and the relationship between optical fields and carrier distributions. Thus, to enable an impact on the SDM system, single VCSELs with multiple individually controllable modes should be developed instead of employing various VCSELs. This approach can largely simplify or even eliminate the need for SMUXs.

In this context, we present our proposal and experiment to etch an air gap directly from the top of the VCSEL mesa to realize two-mode emission of an oxide-confined VCSEL. The upper mesa was separated into two waveguides, each of which was then deposited with p-type contacts. Highly inhomogeneous carrier distributions in the active aperture were expected and observed indirectly when a current was injected from only one contact with only one mode emitting from beneath. For the two-contact-biased condition, two different spatial modes were simultaneously stimulated and emitted from different sub-mesas.

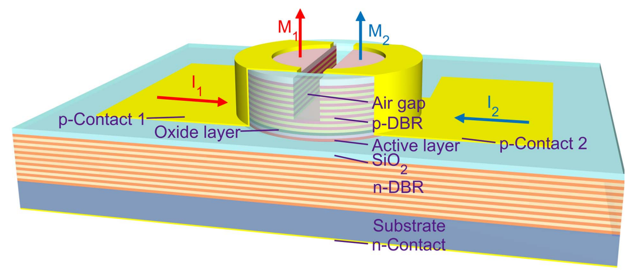

Fig. 1. Three-dimensional sketch of the two-mode VCSEL with an air gap etched in the upper p-doped distributed Bragg reflector layers. When current I_1 is injected through p-Contact 1, mode 1 (M_1) emits. When current I_2 is injected through p-Contact 2, mode 2 (M_2) emits.

II. Device Design & Fabrication

The schematic diagram of our emission-controllable VCSEL emitting nominally at 850 nm is illustrated in Fig. 1. The fabrication process for our device is the same as that of a normal VCSEL, except that an additional step of air gap etching is performed through inductively coupled plasma (ICP) etching immediately after the wet-thermal oxidation. The upper mesa is divided into two lobes with p-contacts deposited above them as depicted in Fig.2 (a). In a conventional VCSEL, the confinement of the carriers and the optical fields is achieved by means of an oxide aperture. In our design, the air gap provides an extra current block and carrier-distribution

Manuscript received August 3, 2017; revised August 26, 2017; accepted September 11, 2017. Date of publication September 18, 2017; date of current version October 13, 2017. This work was supported in part by the National Basic Research Program of China under Grant 2014CB3400102, in part by the National Natural Science Foundation of China under Grant 61434005, Grant 61474118, Grant 61376070, Grant 11404326 and Grant 11674314, and in part by the Youth Innovation Promotion Association, CAS, under Grant 2017260. *(Corresponding author: Lijuan Yu.)*

C. Zhong is with the State Key Laboratory of Luminescence and Applications, Changchun Institute of Optics, Fine Mechanics and Physics, Changchun 130033, China, and also with the University of Chinese Academy of Sciences, Beijing 100049, China (e-mail: zhongchuyu@whu.edu.cn).

X. Zhang, Y. Ning, and L. Wang are with the State Key Laboratory of Luminescence and Applications, Changchun Institute of Optics, Fine Mechanics and Physics, Changchun 130033, China (e-mail: zhangx@ciomp.ac.cn; ningyq@ciomp.ac.cn; wanglj@ciomp.ac.cn).

L. Yu and J. Liu are with the State Key Laboratory of Integrated Optoelectronics, Institute of Semiconductors, Chinese Academy of Sciences, Beijing 100083, China (e-mail: ylj@semi.ac.cn; jgliu@semi.ac.cn).

W. Hofmann is with the Institut für Festkörperphysik und Zentrum für Nanophotonik, Technical University of Berlin, 10623 Berlin, Germany (e-mail: werner.hofmann@tu-berlin.de).

Color versions of one or more of the figures in this letter are available online at http://ieeexplore.ieee.org.

Digital Object Identifier 10.1109/LPT.2017.2753320

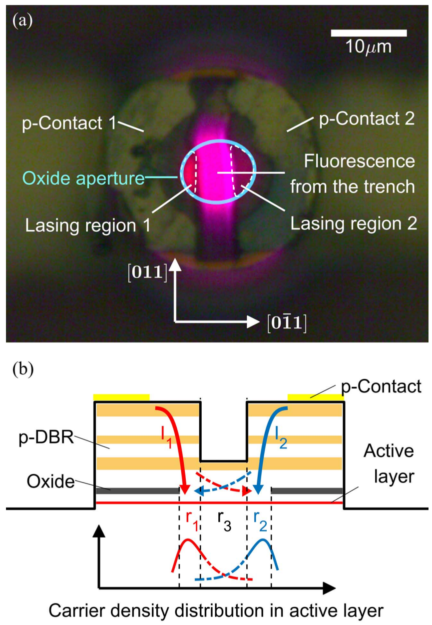

Fig. 2. (a) Microscope image of the output window of the mode-controllable VCSEL below threshold. (b) Schematic cross section, current flow and carrier density distributions in the active layer of the device. In the active aperture, r_1: lasing region 1 corresponds to M_1, r_2: lasing region 2 corresponds to M_2, r_3: region 3 corresponds to area under the trench . Red curves and arrows stand for p-contact 1 biased condition while the blue ones stand for p-contact 2 biased condition. Dashed arrows and curves stand for currents transferring between two sub-mesas and carriers that do not produce laser.

guidance, as shown in Fig. 2(b). The trench enables an inhomogeneity of the carrier distribution in the active region so that different spatial mode emissions can be selected. The width and position of the air trench directly predetermine the sizes of active regions r_1, r_2 and r_3, and the depth influences the inhomogeneity. Fluorescence emits from r_3 because of the low reflectivity above, whereas laser light emits from r_1 and r_2. Besides, the air trench undertakes the functionality of optical restriction. The depth of the trench of our device is approximately 1.8 μm, whereas the depths of the oxide layer and the active layer are 2.9 and 3.1 μm respectively. The width of the air gap is 4.6 μm taking into account that a strong mode coupling may occur between two sub-mesas with a narrower air gap. The direction of the air gap is along the [011] crystal axis. Lastly, because of the anisotropy of oxidation speed of the oxide layer, the oxide aperture has an elliptical shape, with a major axis at an oblique angle to the [011] crystal axis. Fabrication imperfections lead to the trench being slightly off-centered. Consequently we obtain two lasing regions with unique geometrical shapes, as shown in Fig.2 (a).

III. Experimental Results

The tested device has an elliptical oxide aperture with major and minor axes of approximately 9.86 and 9.0 μm respectively, which is smaller than a few-mode fiber's core or a multi-mode fiber's core. Measurements were performed under continuous-wave operation at room temperature and three kinds of injection conditions, namely, I_1 injection (only Contact 1 is biased), I_2 injection (only Contact 2 is biased) and two-contact injection(both contacts are biased).

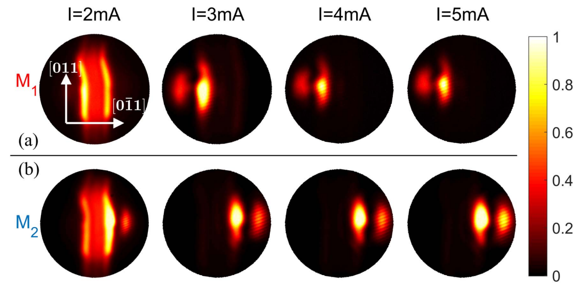

Fig. 3. Near-field patterns of M_1 and M_2 in (a) I_1 injection and (b) I_2 injection. The profile of the air gap can be seen at 2-mA injection.

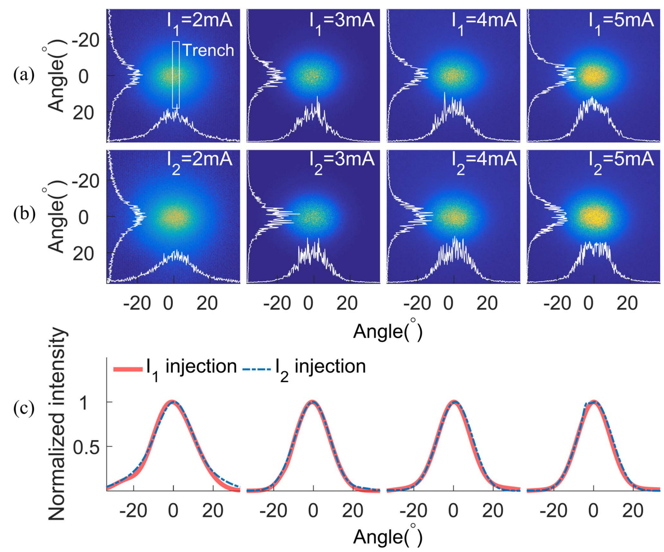

Fig. 4. Far-field profiles and profile cuts in major and minor field axes of M_1 and M_2 in (a) I_1 injection and (b) I_2 injection. (c) Gaussian fits of profile cuts orthogonal to the trench.

As expected, I_1 injection only led to mode M_1 emission and I_2 injection only led to mode M_2 emission (Fig. 3). Distinct parallel-bar-shaped fluorescence patterns emerged from the air gap at 2 mA in both injections, from which a certain degree of deformation of the air gap is observed. At increased driving currents, the laser modes in two single-contact injections exhibited an apparent centrosymmetry instead of a mirror symmetry, which is the result of the angle between the major axis of the aperture and the trench. The abnormal shapes of the near-field profiles can be explained by the irregular shapes of the lasing regions shown in Fig. 2(a). The interference patterns revealed in the emission spots are due to the optical system employed to obtain near-field profiles. We note that neutral density filters of various extinction ratios were used to avoid saturating the charge-coupled-device camera by the laser near-field intensities. Therefore, although the fluorescence from the trench existed upon all the injections, it is nearly invisible at 3, 4 and 5 mA. Far-field profiles and profile cuts are shown in Figs. 4(a) and (b), which has an oblong shape because fluorescence emits from both the trench and the lasing region on the unbiased side. The peak positions of the far-field profiles locate toward the biased side coinciding with the near-field patterns, as shown in the Gaussian fits in Fig. 4(c).

The spectra in the I_1 and I_2 injections are illustrated in Fig. 5 and more detailed spectral information are summarized

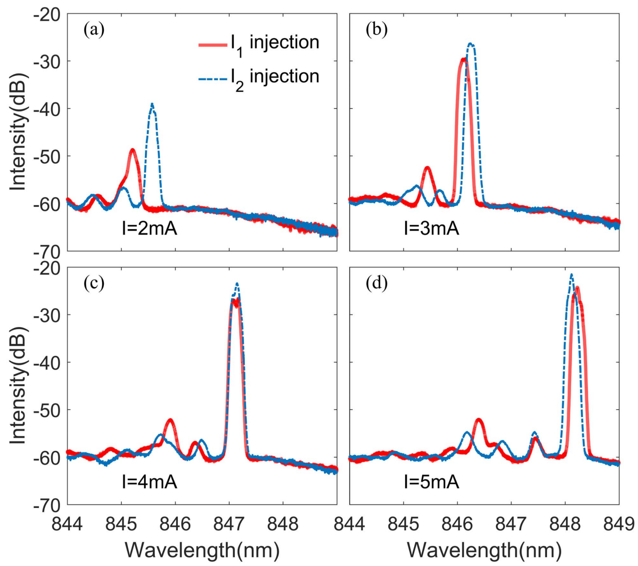

Fig. 5. Spectra of the device in I_1 and I_2 injection under different driving currents.

TABLE I

SPECTRAL CHARACTERISTICS IN DIFFERENT INJECTION CONDITIONS

	Current(mA)	2	3	4	5
I_1	λ_{M_1}(nm)	845.22	846.14	847.12	848.24
	SMSR(dB)	9.63	22.92	25.51	27.8
I_2	λ_{M_2}(nm)	845.56	846.26	847.10	848.12
	SMSR(dB)	16.62	29.91	31.8	33.21
$\Delta\lambda_{M_1,M_2}(\lambda_{M_1}-\lambda_{M_2})$		-0.34	-0.12	0.02	0.12

in Table I. At the same driving currents, the spectra of M_1 and M_2 presented a high degree of similarity and had nearly the same peak wavelength at 4 mA. The VCSEL stays single-mode with a side-mode suppression ratio (SMSR) of about 30 dB in I_2 injection under driving currents larger than 3mA. However, a weaker single-mode operation in I_1 injection can be seen from the spectra of M_1 with stronger secondary peaks and weaker major peaks. Furthermore, the central wavelength of $M_1(\lambda_{M_1})$ increased faster than λ_{M_2} with increasing current, indicating that the thermal resistance of the M_1 side was larger than that of the M_2 side [15].

The differences between M_1 and M_2 in terms of the spectral characteristics and the near-field profiles show that the air gap was displaced to the M_1 side. This can directly be seen from Fig 2.(a) and also partly be deduced from Fig 5.(a) where M_2 shows a much higher major peak. This suggests that the M_2 side has a smaller threshold, which is the expected scenario when displacement of the air gap takes place. This is because the sizes of r_1 and r_2 determine the number of injected carriers that can stimulate laser emissions. In the single-contact injection conditions, the overlap of the carrier distribution with r_1 or r_2 is smaller when one side is smaller than the other. This condition increases the amount of current that is required for lasing. The comparison of the spectra and the transverse modes between the two injection conditions indicate that M_1 and M_2

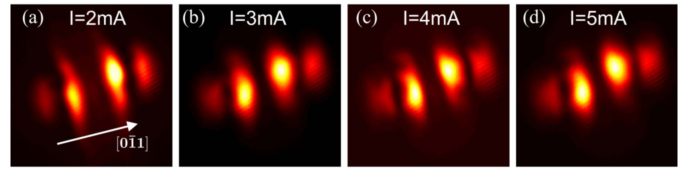

Fig. 6. Near-field profiles of the device in two-contact injection where I_1=I_2=(a) 2 mA, (b) 3 mA, (c) 4 mA, and (d) 5 mA.

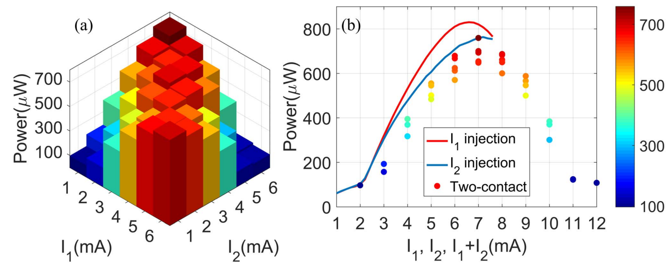

Fig. 7. (a) Output power for two-contact injection. (b) Output power for I_1 injection, I_2 injection (solid lines) and two-contact injection(data points). The x-coordinate of each data point in (b) is the summation of I_1 and I_2 in each (x,y) coordinate, i.e. (I_1, I_2) in (a).

are the same transverse mode solutions of the two symmetric waveguides separated by the air gap. Furthermore, we have achieved independent mode-control of two transverse modes using two different contacts.

The transverse mode in the two-contact injection was further investigated, and the results are shown in Fig. 6. Two-mode emission was then realized. The near-field profiles revealed a centrosymmetry as mentioned, i.e. the near-field profiles highly resemble the ones rotated by 180°. Notably, the VCSEL lases upon a 2-mA two-contact injection. This behavior was not observed under a 2-mA single-contact injection. This result can be an evidence of current transfer under the gap and indicates that the gap was insufficiently deep. Most importantly, our device was verified to have three kinds of operational states, i.e. M_1 operation, M_2 operation, and two-mode operation. The operational state can be switched from one to another. To have a more complete and rigorous understanding of the modal characteristics of our specially designed VCSEL, a fully vectorial optical solver [16], [17] is needed, which would be an extension of our present work.

The light-versus-current (LI) characteristics are illustrated in Fig. 7. Fig. 7(a) shows the three-dimensional bar diagram of the output powers for two-contact injection. Thermal rollover appears near where $I_1 + I_2 = 7$ mA, which is more clearly depicted in Fig. 7(b). From Fig. 7(b), the threshold currents I_{th} in both I_1 injection and I_2 injection are close to 2.2 mA. The LI curves for these two independent injection conditions are very similar to each other until the current exceeds 3mA. The output power in I_1 injection peaks at 830 μW upon 6.6 mA, while the output power of I_2 injection reaches a smaller maximum of 763 μW upon a larger current of 7.2 mA. Compared with I_1 and I_2 injections, two-contact injection shows similar LI characteristics - a similar threshold of 2 mA and a thermal rollover at a total injection current of approximately 7 mA, as noted in Fig. 7(a).

IV. CONCLUSION

We have introduced a VCSEL with two transverse modes individually controllable by two independent contacts deposited on two sides of the mesa. The mesa is cut into two parts by an air gap directly etched through ICP etching. The air gap is designed to achieve current guidance and optical field restriction. Our result indicated that the air gap is functioning. Near-field and far-field profiles and optical spectra under single-contact injection and near-field profiles under two-contact injection, indicate that this device can emit two transverse modes with a high level of symmetry and can be switched from single-mode operation to two-mode operation. In summary, this mesa-cutting method can achieve two-mode formation and control without undergoing a complicated fabrication process. Thus, prospective multiple-spatial-mode operation can be implemented, especially when we increase the number of air gaps similar to cake-cutting and expand the oxide aperture. In addition, the mesa shape, the air gap, and the p-contacts can also be modified to create different spatial modes. There will be a great application prospect to create a new kind of laser sources for SDM-based optical communications.

REFERENCES

[1] K. Szczerba, P. Westbergh, M. Karlsson, P. A. Andrekson, and A. Larsson, "70 Gbps 4-PAM and 56 Gbps 8-PAM Using an 850 nm VCSEL," *J. Lightw. Technol.*, vol. 33, no. 7, pp. 1395–1401, Apr. 1, 2015.

[2] D. M. Kuchta *et al.*, "A 71-Gb/s NRZ modulated 850-nm VCSEL-based optical link," *IEEE Photon. Technol. Lett.*, vol. 27, no. 6, pp. 577–580, Mar. 15, 2015.

[3] A. Amphawan and Y. Fazea, "Laguerre-Gaussian mode division multiplexing in multimode fiber using SLMs in VCSEL arrays," *J. Eur. Opt. Soc.-Rapid Publications*, vol. 12, no. 1, p. 12, Sep. 2016.

[4] B. Zhu, T. F. Taunay, M. F. Yan, M. Fishteyn, G. Oulundsen, and D. Vaidya, "70-Gb/s multicore multimode fiber transmissions for optical data links," *IEEE Photon. Technol. Lett.*, vol. 22, no. 22, pp. 1647–1649, Nov. 15, 2010.

[5] N. Grote, M. Möhrle, and M. Ortsiefer, *Laser Components*. Cham, Switzerland: Springer, 2017, pp. 103–149.

[6] A. Chralyvy, "Plenary paper: The coming capacity crunch," in *Proc. 35th Eur. Conf. Opt. Commun.*, Sep. 2009, p. 1.

[7] P. J. Winzer, "Making spatial multiplexing a reality," *Nature Photon.*, vol. 8, pp. 345–348, Apr. 2014.

[8] D. Richardson, J. Fini, and L. Nelson, "Space-division multiplexing in optical fibres," *Nature Photon.*, vol. 7, no. 5, pp. 354–362, 2013.

[9] A. Larsson, P. Westbergh, J. S. Gustavsson, E. Haglund, and E. P. Haglund, "High-speed VCSELs and VCSEL arrays for single- and multi-core fiber interconnects," *Proc. SPIE*, vol. 9381, p. 93810D, Mar. 2015.

[10] C. Xie *et al.*, "400-Gb/s PDM-4pam WDM system using a monolithic 2×4 VCSEL array and coherent detection," *J. Lightw. Technol.*, vol. 33, no. 3, pp. 670–677, Feb. 1, 2015.

[11] H. Chen and A. M. J. T. Koonen, *Spatial Division Multiplexing*. Cham, Switzerland: Springer, 2017, pp. 1–48.

[12] C. Degen, W. Elsaber, and I. Fischer, "Transverse modes in oxide confined vcsels: Influence of pump profile, spatial hole burning, and thermal effects," *Opt. Exp.*, vol. 5, pp. 38–47, Aug. 1999.

[13] A. Furukawa, S. Sasaki, M. Hoshi, A. Matsuzono, K. Moritoh, and T. Baba, "High-power single-mode vertical-cavity surface-emitting lasers with triangular holey structure," *Appl. Phys. Lett.*, vol. 85, pp. 5161–5163, Nov. 2004.

[14] P. Debernardi, A. Kroner, F. Rinaldi, and R. Michalzik, "Surface relief versus standard VCSELs: A comparison between experimental and hot-cavity model results," *IEEE J. Sel. Topics Quantum Electron.*, vol. 15, no. 3, pp. 828–837, May 2009.

[15] H. Moench *et al.*, "Advanced characterization techniques for high power VCSELs," *Proc. SPIE*, vol. 7615, p. 76150G, Feb. 2010.

[16] T. Czyszanowski, M. Dems, and K. Panajotov, "Single mode condition and modes discrimination in photonic-crystal 1.3 μm AlInGaAs/InP VCSEL," *Opt. Exp.*, vol. 15, pp. 5604–5609, Apr. 2007.

[17] M. Dems, I.-S. Chung, P. Nyakas, S. Bischoff, and K. Panajotov, "Numerical methods for modeling photonic-crystal vcsels," *Opt. Exp.*, vol. 18, p. 16042, Jul. 2010.